Chemical Engineering Science 66 (2011) 2453–2467

Contents lists available at ScienceDirect

Chemical Engineering Science

journal homepage: www.elsevier.com/locate/ces

Interrogating the effect of 90° bends on air–silicone oil flows using advanced instrumentation

M. Abdulkadir, D. Zhao, S. Sharaf, L. Abdulkareem, I.S. Lowndes, B.J. Azzopardi *

Process and Environmental Engineering Research Division, Faculty of Engineering, University of Nottingham, University Park, Nottingham NG7 2RD, UK

ARTICLE INFO

Article history:
Received 26 September 2010
Received in revised form
27 January 2011
Accepted 9 March 2011
Available online 15 March 2011

Keywords:
Gas/liquid
Bend
Electrical tomography
Capacitance
Void fraction
Flow regime

ABSTRACT

When gas/liquid mixtures flow around a bend they are subjected to forces additional to those encountered in a straight pipe. The behaviour of the flows at the inlet and outlet of the bend depends on the orientation of the pipes. Air/silicone oil flows around a 90° bend have been investigated using advanced instrumentation: Electrical Capacitance Tomography (ECT), Wire Mesh Sensor Tomography (WMS) and high-speed video. The first two provide time and cross-sectionally resolved data on void fraction. ECT probes were mounted 10 diameters upstream of the bend whilst WMS was positioned either immediately upstream or immediately downstream of the bend. The downstream pipe was maintained horizontal whilst the upstream pipe was mounted either vertically or horizontally. The bend ($R/D=2.3$) was made of transparent acrylic resin. From an analysis of the output from the tomography equipment, flow patterns were identified using both the reconstructed images as well as the characteristic signatures of Probability Density Function (PDF) plots of the time series of cross-sectionally averaged void fraction as suggested by Costigan and Whalley (1996). The superficial velocities of the air ranged from 0.05 to 4.73 m/s and for the silicone oil from 0.05 to 0.38 m/s. Bubble/spherical cap, slug, unstable slug and churn flows were observed before the bend for the vertical pipe and plug, slug, stratified wavy and annular flows when the pipe was horizontal. Bubble, stratified wavy, slug, semi-annular and annular flows are seen after the bend for the vertical 90° bend whilst for the horizontal 90° bend, the flow patterns remained the same as before the bend. Flow patterns for the vertical and horizontal 90° bends are shown on the diagram of the gas superficial velocity versus liquid superficial velocity. These results are confirmed by the high-speed videos taken around the bend. A previously proposed criterion, to determine stratification after the bend, based on a modified Froude number have been shown to be valid for a liquid different from that tested in the original paper.

1. Introduction

Production and transportation engineers in the onshore and offshore oil and gas industries have always been facing technical and environmental challenges associated with multiphase flows. For example, in an offshore environment, it is economically preferable to transport both gas and liquid through a single flowline and separate them onshore. In this way, a significant cost can be saved by eliminating the separate pipelines and phase separators at the offshore platform of Floating Production and Storage Operation. Hitherto, applications in the petroleum industry provide another strong motivation for multiphase flow research. However, the instability problems caused by the multiphase flow can ultimately damage the pipeline system and this is unacceptable. The pipeline geometry contains not just straight pipes but also fittings such as, bends, valves, junctions and other fittings, which make the flow gas and liquid more complicated. These fittings may lead to secondary flow, strongly fluctuating void fractions, flow excursions, flow separation, pressure pulsations and other unsteady flow phenomena. These phenomena can cause problems such as burn-out, corrosion and tube failure, resulting in expensive outages, repairs and early replacement affecting plant reliability and safety. Among these fittings, bends are often encountered in oil/gas production system because of: terrain undulation; flowline/riser combinations and at delivery points to production facilities. The presence of a bend can drastically change the flow patterns downstream of it particularly immediately downstream. It is in view of this that it is of major interest to a wide range of industrial processes that employ pipeline transport systems. Also the requirements for economic design, optimization of operating conditions and evaluation of safety factors create the need for quantitative information about such flows. As the capital and operating costs become competitive and the importance of reliability increases, the need for accurate

* Corresponding author.
E-mail address: barry.azzopardi@nottingham.ac.uk (B.J. Azzopardi).

0009-2509/$ - see front matter © 2011 Elsevier Ltd. All rights reserved.
doi:10.1016/j.ces.2011.03.006

information becomes even more important. Unfortunately, the flow redistribution phenomenon in bends, however, has received little attention. Literature on this subject is very limited. Most of the investigations have been restricted to single-phase flow (Eustice, 1910; Dean, 1927, 1928; Jayanti, 1990; Dewhurst et al., 1990; Spedding et al., 2004). A few papers, such as Gardner and Neller (1969), Oshinowo and Charles (1974), Carver (1984), Carver and Salcudean (1986), Ellul and Issa (1987), Legius and van der Akker (1997), Azzi et al. (2002), Azzi and Friedel (2005), Spedding and Benard (2006) and Shannak et al. (2009), address the issue of gas–liquid systems but some of their experiments are confined to pipes of diameters much smaller than those used in industry. In addition, the physical properties of the fluids employed are very different from those dealt with by industry.

1.1. Gas–liquid flow in bends

Two-phase flow patterns observed in bends are qualitatively the same as those seen in straight pipes. However, bends introduce a developing situation in the flow pattern, whereby the relative positions and local velocities of the two phases are redistributed.

Gardner and Neller (1969) carried out visual and experimental studies for bubble/slug flow using a transparent pipe of 76 mm diameter in a vertical 90° bends of 305 and 610 mm radii of curvature, using air–water at atmospheric pressure. The local air concentrations over chosen cross-sections were measured. Their experimental data were used to interpret the effect of the competition between centrifugal and gravity forces on the flow distribution in bends. They suggested that the ratio of centrifugal and gravitational forces can be represented by a modified Froude number. They found out that gas can either flow on the inside or outside of the bend depending on a critical Froude number defined as

$$Fr_\theta = \frac{U_m^2}{Rg\sin\theta} \tag{1}$$

where U_m is the mixture velocity and θ is the angle of the bend. With this Froude number, they attempted an explanation for phase positions. They claimed that if Fr_θ is greater than unity, air will be found on the inside of the bend, and if less than unity, air will hug the outside of the bend. $Fr_\theta=1$ corresponds to both phases being in radial equilibrium. This conclusion, however, may not be valid for working liquids with different viscosity, density and surface tension.

Carver (1984) carried out numerical work on the vertical 90° bend using a 2-Dimensional (D) numerical computation method. They compared their results with those of Gardner and Neller (1969). The agreement was not particularly good. Carver and Salcudean (1986) recognized the limitations of using the 2-D numerical approach to simulate truly 3-D flows. They extended the 2-D model to 3-D and found that the 3-D model can give the similar trend as observed by Gardner and Neller (1969). Ellul and Issa (1987) developed an improved 3-D simulation where substantially different solution algorithm was adopted, a truncated gas momentum was added into their momentum equations and both air–water and gas–oil mixtures were considered. The simulation results showed better agreement with the experimental data than those obtained by the 2-D model in Carver (1984). No grid sensitivity analysis was reported in the work of Ellul and Issa (1987). The simulation result could not select the optimum mesh size. No experimental data was available at that time for them to validate their gas–oil simulation.

Legius and van der Akker (1997) carried out a numerical and experimental study in a bend of 630 mm radius of curvature using air–water at atmospheric pressure. The experimental facility consisted of a transparent acrylic horizontal flowline (9 m long) connected to a vertical riser (4 m in height) by the 630 mm radius bend. The diameter of all pipes was 100 mm. Visual observation: 200 Hz digital camera and an Auto-regressive modelling method were used for flow regime identification. Slug and churn flow in the riser and stratified, slug and a new regime called "geometry enhanced slugging" in the flowline were identified. The time dependent behaviour of two-phase flow was modelled by an in-house code named Solution Package for Hyperbolic Functions (SOPHY-2). Good agreement between modelling and experiment results has been found under almost all conditions except at higher gas and lower liquid flow rates. However, the information presented for the characteristics of slug flow is limited. Important

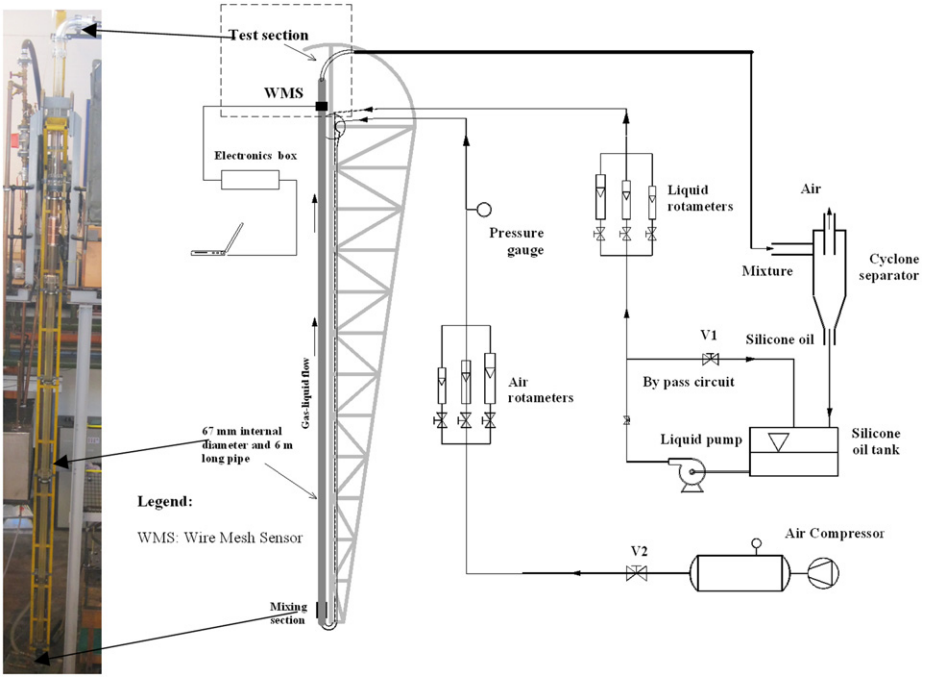

Fig. 1. Schematic diagram of inclinable rig.

parameters like void fraction in liquid slug and Taylor bubble were not presented. The dependence of the Taylor bubbles and liquid slugs on the gas flow rates was not examined. The sample frequency of 50–100 Hz used by these researchers seems too slow to get good spatial resolution of signals.

It can be concluded that most of the work reported in the literature on the multiphase flow in bends were carried out in small diameter pipes with air–water as the model fluids. Emphasis was on the determination of the pressure drop and phase distribution inside the bends. The change of flow structure before and after the bends was mainly obtained by visualization and the underlining mechanism for the change of flow patterns was not discussed. For that reason, it is important to study the effect of bends on two-phase flow in more industry relevant fluids for the optimal, efficient and safe design and operation of the flow systems. This paper is aimed to provide a more complete understanding on the flow phenomenon occurring in bends through the comprehensive experimental investigation in both vertical and horizontal pipes. The examined fluids are air and silicone oil. Advanced instruments such as Electrical Capacitance Tomography (ECT), Wire Mesh Sensors (WMS) and high speed video camera have been used to measure void fractions before and after the bend. The flow patterns were determined by analyzing the Probability Density Function (PDF) of the time series of void fractions. This analysis was validated by the flow visualisation in the bend with the aid of a high speed video camera. With this information a more fundamental approach is used for improving the general knowledge on the effect of 90° bends on two-phase flow.

2. Experimental facility and procedure

All experiments were carried out in an inclinable rig, shown in Fig. 1. The experimental facility consists of a main test section of the rig made from transparent acrylic resin pipes of 67 mm inside diameter and 6 m long to allow for flow development over the test section. The rigid steel frame supporting the test pipe is set-up so that it can be inclined from −5° to 90° at intervals of 5°, to enable investigation of the influence of different inclinations on flow patterns. In this paper only the experimental results obtained at the vertical and horizontal positions are discussed.

Air was supplied from laboratory compressed air main and measured by one of two variable area metres mounted in parallel. In addition, the static pressure of air was measured prior to entering the mixing section. Liquid was taken from a liquid storage tank and pumped by a centrifugal pump and metered by one of two variable area metres mounted in parallel. Air was mixed with liquid at the mixer before the mixture entered into the straight pipe, passed through a 90° bend and finally goes to a separator where air was released to the atmosphere from the top and liquid, under the influence of gravity, returned to main liquid storage. More details can be found in Abdulkadir et al. (2010).

A 90° bend with a radius of curvature of 0.15 m was mounted at the end of the straight pipe as shown in Fig. 2. Downstream of the bend there is another straight pipe from which the gas–liquid mixture enters a flexible pipe that takes it to the phase separator. Two bend positions were investigated: (1) vertical bend (upstream – vertical riser/downstream – horizontal flowline) and (2) horizontal bend (upstream – horizontal flow lines upstream/and downstream). The behaviour of the air–silicone oil mixture was examined using ECT and WMS.

A detailed description of the theory behind the ECT technology is described by Hammer (1983), Huang (1995), Zhu et al. (2003), Hunt et al. (2004) and Hernandez Perez et al. (2010). The method can image the dielectric components in the pipe flow phases by

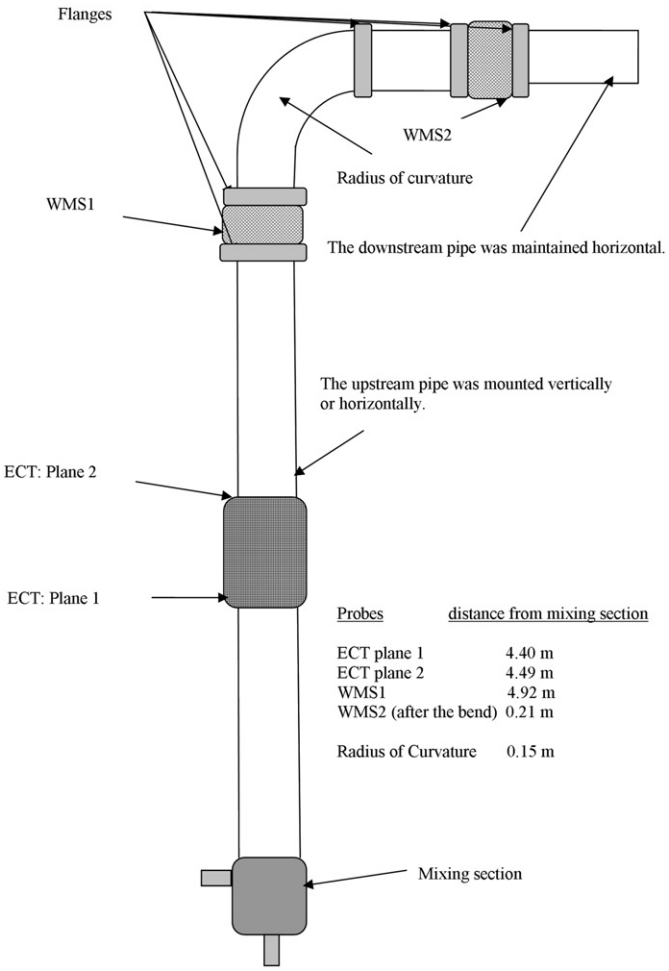

Fig. 2. Schematic diagram of vertical 90° bend.

measuring rapidly and continually the capacitances of the passing flow across several pairs of electrodes mounted uniformly around an imaging section. Thus, the sequential variation of the spatial distribution of the dielectric constants that represent the different flow phases may be determined. In this study, a ring of electrodes were placed around the circumference of the riser at a given height above the mixer at the bottom of the 6 m riser section. This enabled the measurement of the instantaneous distribution of the flow phases over the cross-section of the pipe.

The capacitance WMS technology, described in detail by da Silva et al. (2010) can image the dielectric components in the pipe flow phases by measuring rapidly and continually the capacitances of the passing flow across several crossing points in the mesh. It consists of two planes of 24 stainless steel wires with 0.12 mm diameter, with a 2.78 mm wire separation within each plane and 2 mm axial plane displacement. This determined the spatio/temporal resolution of the sensor. Since the square sensor is installed in a circular tube, only 440 of the total 576 wire crossing points are within the radius of the tube Abdulkadir et al. (2010). During the experiments, the transmitter lines are pulsed one after another. By measuring the signal of all crossing orthogonal receiver wires, the local capacitance at the crossing points in the mesh is determined. This capacitance signal is a measure for the amount of silicone oil, and thus indicates the local phase composition in the grid cell.

ECT was placed 4.49 m (67 diameters) away from the mixing section while WMS was first placed at about 4.92 m (73 diameters) away from the mixing section. WMS was afterwards

moved to a distance of about 0.21 m (3 diameters) after the bend. The experiments were performed at room temperature (15–20°). The properties of the two fluids used in the experiments are as shown in Table 1. The influence of the bend orientation on the flow behaviour was studied by changing the position of the inlet pipe from vertical to horizontal.

2.1. Testing of instruments

Advanced instruments, ECT and WMS involve using tomographic imaging methods to manipulate data from remote sensors in order to obtain precise quantitative information from inaccessible locations. The need for this instrumentation is analogous to the medical need for body scanners, which has been met by the development of computer-aided tomography.

In this work, WMS was used to give detailed information about air–silicone flows while ECT as a check on the void fraction measurement accuracy. It presents results of testing carried out to give ourselves confidence in the results presented by the instruments. Measurements have been made with the aid of the instrumentation at a liquid superficial velocity of 0.05–0.38 m/s and for air flow rates in the range 0.05–4.73 m/s air described above. WMS electronics was used to trigger ECT electronic so results were exactly simultaneous. The sampling frequencies for ECT and WMS were 200 and 1000 Hz, respectively. A great deal of information can be extracted by examining the time series of cross-sectionally averaged void fraction. In particular, the probability density function (PDF) of these void fractions can have characteristic signatures. The results of the PDF of void fraction were further reinforced by the cross-sectional slice view of void fraction obtained from WMS. Fig. 3 shows the PDF of void fraction from ECT and WMS. The figure illustrates the agreement between the two methods of measurements.

Table 1
Properties of the fluids.

Fluid	Density (kg/m^3)	Viscosity (kg/ms)	Surface tension (N/m)
Air	1.18	0.000018	–
Silicone oil	900	0.0053	0.02

2.1.1. Comparison of PDFs of void fraction for ECT and WMS for the riser before the vertical 90° bends

Fig. 3a–c presents the comparison between the PDFs of void fraction for ECT and WMS for same flow conditions in a vertical riser. The plots show that at a liquid superficial velocity of 0.05 m/s and a gas superficial velocity of 0.05 m/s, both ECT and WMS identify the flow regime as spherical cap bubble. However, ECT provides a higher peak value while WMS predicts higher void fraction. Increasing the gas superficial velocity to 0.54 m/s whilst maintaining same liquid velocity of 0.14 m/s the characteristic signature of the flow regime according to both ECT and WMS is that of slug flow. It can also be observed that ECT still provides higher PDF of void fraction than WMS but with a lesser range compared to at gas superficial velocity of 0.05 m/s while WMS provides a higher void fraction. At a gas superficial velocity of 4.73 m/s, ECT and WMS both defined the flow pattern as churn flow. It is interesting to note that both the PDF of void fraction for ECT and WMS show almost the same peak. The degree of agreement of the length of the PDF and void fraction improves with an increase in gas superficial velocity. The result therefore shows that both instruments predict the similar signatures.

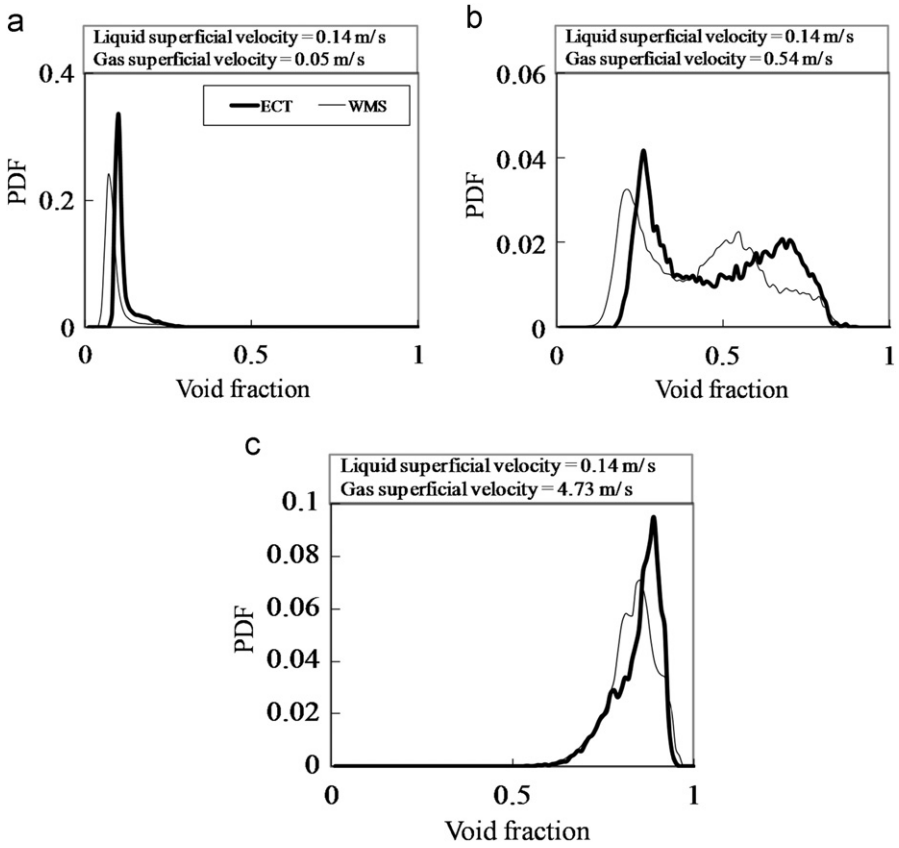

Fig. 3. Comparison of PDFs of void fraction for ECT and WMS before the vertical 90° bend.

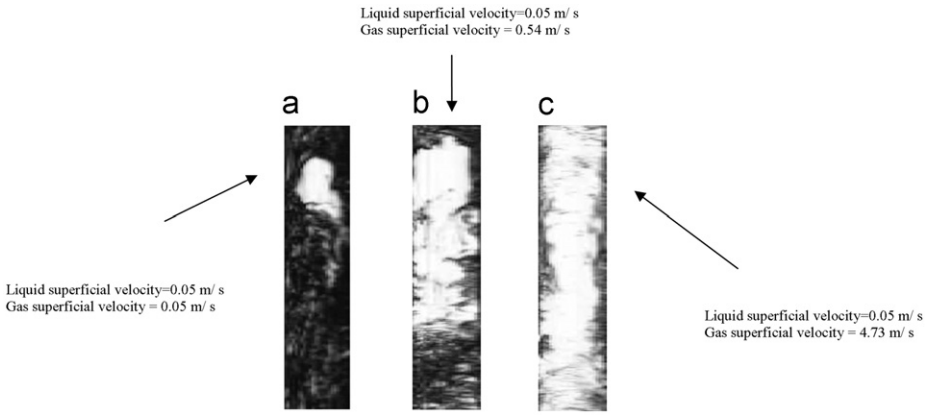

Fig. 4. Reconstructed images of two-phase flow patterns from spherical cap bubble to churn flow.

2.1.2. Reconstructed images of the two-phase flow before the vertical 90° bends as depicted by WMS

Fig. 4a–c shows 2 diametric slice views for the void fractions observed for different gas superficial velocities, which support the result obtained in Fig. 3a–c. At a gas superficial velocity of 0.05 m/s, there are still bubbles of large size, but not as big as the pipe diameter. These are often described as spherical cap bubble. When the gas velocity is increased to 0.54 m/s, coalescence starts leading to slug flow. At gas superficial velocity of 4.73 m/s, the slug flow has been changed to churn flow. This results obtained are in agreement with the results obtained in Fig. 3a–c.

3. Results and discussion

Several runs were carried out with air–silicone oil mixture mainly for the purpose of defining and classifying all the two-phase flow patterns attainable with the experimental rig using ECT and WMS. The liquid superficial velocities investigated were 0.05–0.38 m/s and gas superficial velocities ranged from 0.05 to 4.73 m/s. In each of these runs, independent visual observations and flow characteristics were recorded in detail for the vertical riser, bends and flowline (horizontal pipe). Comparisons between the flow regimes before and after the bends were made based on the PDF of void fraction. All the flow regimes for the vertical and horizontal 90° bends were then categorized based on the basis of visual observations and supported by high speed video image. A flow pattern map was used to summarize the flow patterns observed in both the vertical and horizontal 90° bends. It was observed that the transition from one flow pattern to another was gradual with respect to fluid flow rates. Comparisons were made of the effect of gas and liquid superficial velocities on mean cross-sectional void fraction distribution, before and after the vertical and horizontal 90° bends. Finally, comparison of present study with the works of Gardner and Neller (1969) will be made based on the modified Froude number.

3.1. Comparison of PDFs of void fraction before and after the bend using WMS

PDF is the rate of change of the probability that void fraction values lie within a certain range ($0 \leq \varepsilon \leq 1$) versus void fraction. The PDF of time varying void fractions has been used to classify the flow patterns in the same manner as Costigan and Whalley (1996) and Omebere-Iyari and Azzopardi (2007). A single peak at low void fraction represents bubble flow and a double peak feature with one at low void fraction whiles the other one at high void fraction represents slug flow. A single peak at low void fraction accompanied by a broadening tail represents spherical cap bubble whiles a single peak at a high void fraction with a broadening tail represents churn flow.

The PDFs of the void fraction data obtained at different liquid superficial velocity of 0.05–0.38 m/s and variable gas superficial velocities from 0.05 to 4.73 m/s are shown in Fig. 5. In the top plot, the PDF for the riser before the vertical bend (the dark curve) are compared with that for the flowline before the horizontal bend (the light curve) at the same flow conditions. The bottom plot gives the same comparison for the scenario after the bend.

One interesting observation made in this study is that the liquid flow rate has little effect on the two-phase flow behaviour for the upstream section of the vertical 90° bend, the flow patterns are substantially the same (cap bubble, slug, unstable and churn flows) irrespective of an increase in the liquid superficial velocity as shown in Fig. 5. There might be small differences in the gas flow at which the transitions occurred. In contrast, for the horizontal 90° degree bend, the liquid flow rate has a noticeable effect on the two-phase flow behaviour. The flow patterns observed at low liquid flow rate, i.e., stratified wavy and annular flows changed to plug and slug flows when the liquid superficial velocity is increased. This is not surprising because the amount of liquid present in the pipe at low liquid superficial velocity is too small for plug or slug flows to exists and as a result, stratified wavy or annular flows are formed. But as the liquid flow rate is increased, plug and slug flows begin to appear.

On the other hand for the downstream section, both the vertical and horizontal 90° bends show the same flow pattern at the lowest liquid superficial velocity (0.05 m/s) and highest gas superficial velocity (4.73 m/s) as illustrated in Fig. 5. The flow pattern downstream of both bends is annular. This is supported by direct visual observations. This behaviour is a result of the impact of the air–silicone oil flow on the bend, splashing some of the liquid to the top and bottom of the pipe. The pipe beyond the Wire Mesh Sensor (WMS) was opaque. However, it is expected that the flow would settle to stratified wavy flow.

At liquid superficial velocity of 0.14 m/s and low gas flow rate (gas superficial velocity = 0.05 m/s), the PDF for the vertical riser presents a single peak of the void fraction value at about 0.06 with a broadening tail extending to a higher value of about 0.35. This defines a spherical cap bubble flow as in Costigan and Whalley (1996) with a velocity higher than the velocity of the small bubbles. The flow pattern has been confirmed by the images of high speed video camera as shown in Fig. 7. The gas bubbles indeed exhibit spherical cap shapes. When the vertical riser was positioned to become horizontal (flowline), the PDF of the void fraction at the same flow rate, shows a dominant peak at 0.14 with a wide base spanning from 0 to 0.36. This is the typical

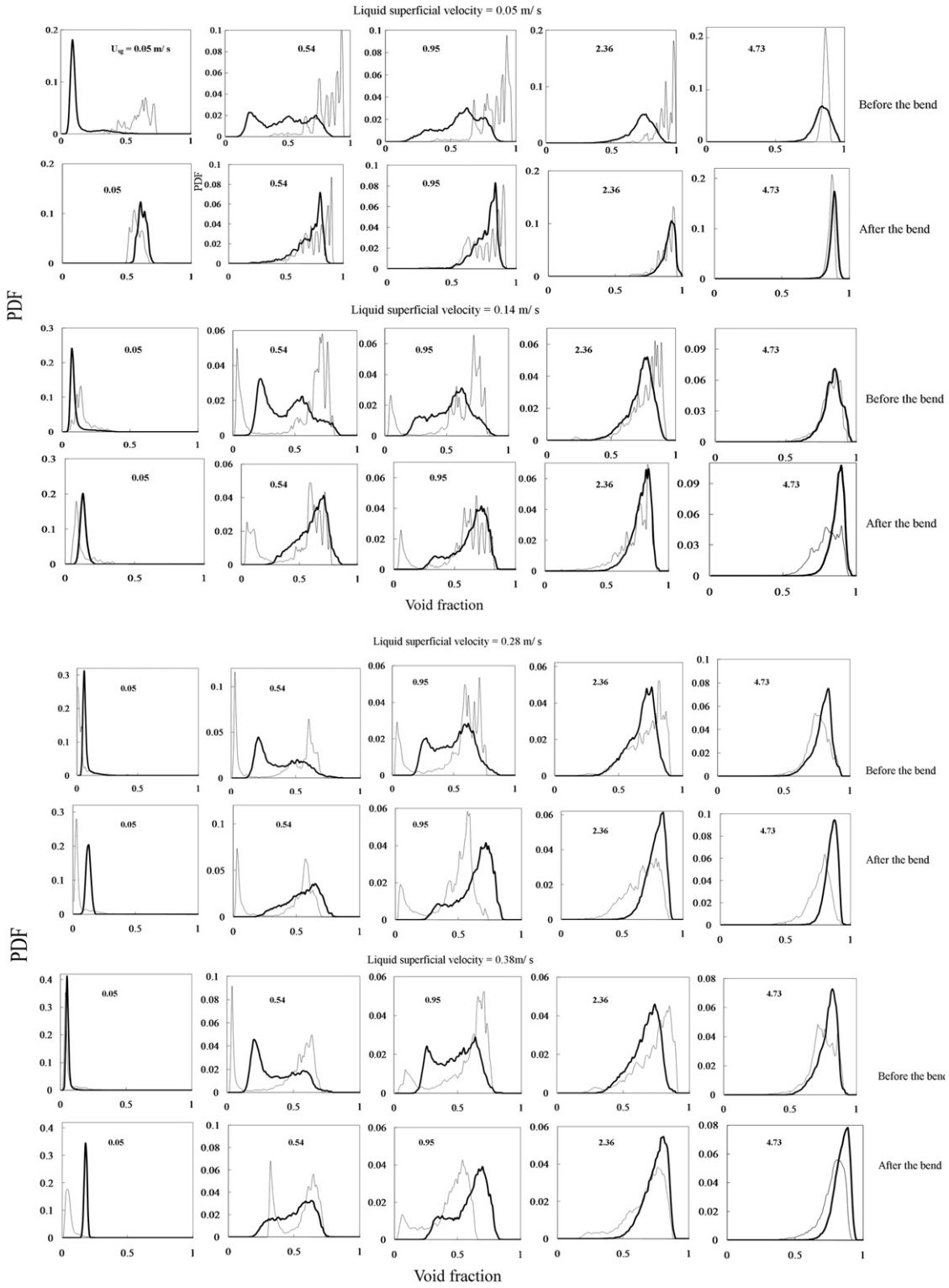

Fig. 5. PDF of void fraction before and after the bend.

feature of plug flow. The elongated gas bubbles are separated by sections of continuous liquid moving downstream along the top part of the pipe with almost zero void fractions in the liquid. The variation of the void fraction reflects the different size of the gas bubbles and the continuous liquid phase. After the bend, the PDF for the horizontal pipe in the riser shows a single peak, the signature of bubbly flow. The broaden tail present in the PDF of the riser does not exist in the PDF after the bend. The big cap bubbles break up in the bend due to the balance of the centrifugal and the surface tension forces. The bubbles become more uniform. For the horizontal arrangement, the PDF after the bend move to the lower void fraction values with the dominant peak frequency at the void fraction of 0.08. There is little change in the size of the wide base compared with that before the bend.

With the same mechanism the elongated bubbles break into smaller bubbles when passing through the bend. The flow patterns are still kept as plug flow though.

When the gas flow rate increases to 0.54 m/s, the cap bubbles coalesce into bullet-shaped Taylor bubbles and a slug flow regime is formed. The PDF of the void fractions in the riser gives two main peaks at the values of 0.22 and 0.55, respectively. These peaks are the signature of the aerated liquid slugs and the Taylor bubbles with the different sizes. Taylor bubbles are not yet fully developed. This is confirmed by the analysis of the video images as shown in Fig. 8. Similar to that for the riser, the PDF for the horizontal flowline has one narrow peak at the value of 0.02 and one wide peak with fluctuations at around 0.7. With the increase in gas superficial velocity from 0.05 to 0.54 m/s, the elongated bubbles grow and coalescence into bullet-shaped Taylor bubbles. The flow pattern changes from the plug flow to the slug flow. After the bend, the PDF of the void fraction in the flowline for the riser has a "hill" shape. Stratified wavy flow was observed. For the horizontal setup, compared with the PDF before the bend, the lower void fraction peak moves to the higher void fraction values and more peaks appear at the void fractions 0.5–0.8. This can probably be attributed to the collapse of the big Taylor bubbles while passing through the bend. However, the flow pattern remained as slug flow.

When the gas flow rate reaches 0.95 m/s, again two peaks appear on the PDF graph of void fractions for the riser but the height of the lower void fraction peak decreases more than 50% while the PDF of the higher void fraction increases more than 40% compared with those at 0.54 m/s. The increase in gas superficial velocity leads to the increase in Taylor bubbles and the shrinkage of the liquid slugs. More and more bubbles are entrained in the liquid slugs. This pattern according to Costigan and Whalley (1996) is defined as unstable slug flow. For the case of the flowline arrangement, the height of the lower void fraction peak also decreases significantly. The PDF curve moves to the higher void fraction values with the increase in the gas superficial velocity. After the bend for the riser setup, with the increase of gas superficial velocity from 0.54 to 0.95 m/s, the stratified wavy flow in the flowline becomes the developing slug flow, which is featured by a small peak superimposed on a big peak with a wide base. With the increase in gas superficial velocity from 0.54 m/s the waves becomes stronger and as consequence more bubbles are trapped inside. At a certain point the Taylor bubbles are formed. For the horizontal setup, no significant difference is present in the PDF between before and after the bend except the significant reduction in the height of the peak at the high void fraction ($\sim$0.72).

At 2.36 m/s, the PDF of void fraction for the riser has a single peak at about 0.76 with broadened tails down to 0.2 and 0.9. This is the typical feature of churn flow. An increase in the gas superficial velocity escalates the instability of liquid slugs. When the speed of gas core reaches to a certain point, the liquid slugs will be penetrated and the integrity of the Taylor bubbles will be destroyed. This leads to the transition to churn flow. For the horizontal setup, released liquid from the collapsed slugs accumulates on the bottom part of the pipe and strong wave caused by the gas travel on the upper part of the pipe. Stratified wavy flow is formed. After the bend, the PDF of the void fractions for the riser significantly shifts to the higher values compared with that before the bend. The dominant void fraction from 0.75 increases to 0.83 and its count increases more than 40%. The churn flow before the bend changes to semi-annular after the bend. This has been confirmed by visualization analysis. The liquid film, however, is erratic and showed some disturbances

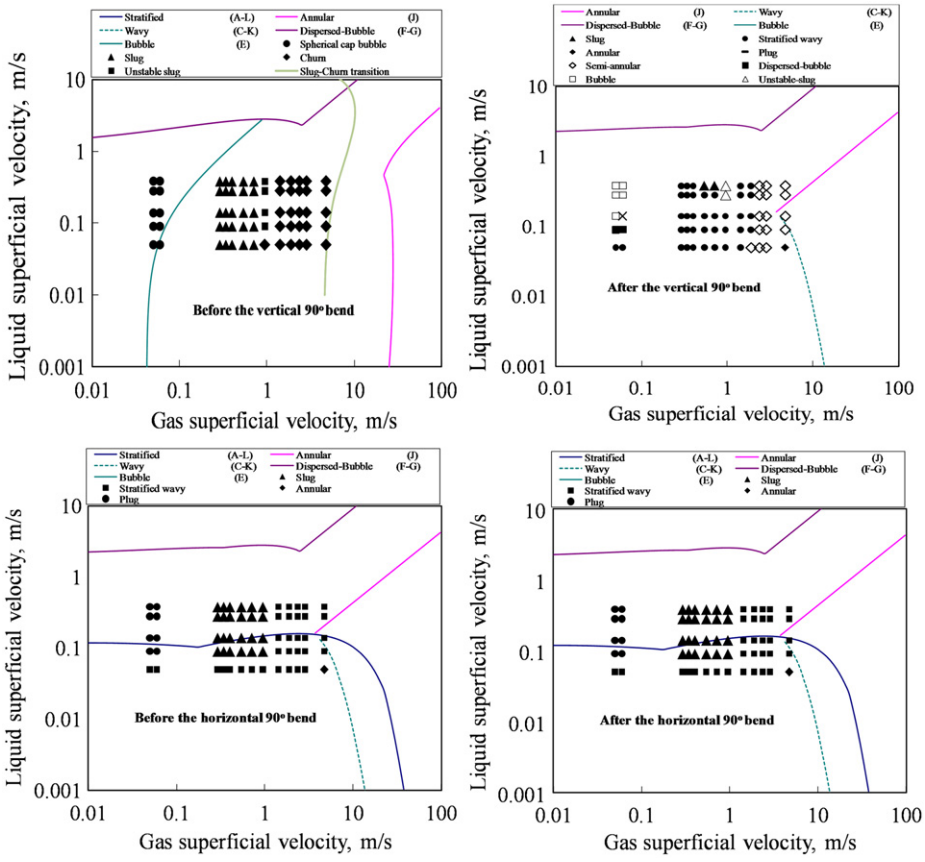

Fig. 6. Flow pattern maps for vertical and horizontal 90° bends.

with void fractions down to about 0.5. For the horizontal arrangement, no significant flow pattern change was observed. It keeps the same stratified wavy after the bend.

At the highest gas flow rate of 4.73 m/s we examined, the PDF of void fractions for the riser has very similar shape to that at 2.36 m/s but with a much narrower tail. The peak moves towards the higher void fraction. The flow pattern is still the churn flow, but close to the transition to semi-annular flow. For the horizontal layout, with the increase of gas flow rate from 2.36 to 4.73 m/s, the liquid film becomes more and more uniformly distributed around pipe wall. This is reflected on the PDF curve where the peak becomes narrower and exhibits less fluctuation. The annular flow regime is approached when the gas superficial velocity is big enough to distribute evenly the liquid on the pipe wall. After the bend, semi-annular flow is present in the flowline for the riser and stratified wavy appears in the flowline for the horizontal arrangements.

A flow pattern map is presented in Fig. 6, summarizing all the flow patterns observed in both the vertical and horizontal 90° bends.

3.2. Flow patterns identification using high speed video images and WMS output

3.2.1. Flow regimes in vertical riser (vertical 90° bend)

Given below are descriptions of the various flow patterns in the order that they might be expected to occur for constant liquid flow rate and increasing air flow rate:

Spherical cap bubble: here, as shown in Fig. 7a, there can be swarms of small bubbles with increase in gas velocity. The bubbles are now forming larger ones, as shown in Fig. 7b, but not big enough to cover the pipe diameter. The velocity of a bubble may differ substantially from that of the liquid phase. At this flow rate, both the bubble number density and the mean diameter of the bubbles increase. The inter-bubble space decreases and the movement of the bubbles become more irregular. Due to the collisions between bubbles, coalescence takes place and spherical cap bubble flow is formed. As a consequence of coalescence and velocity differences, the bubbles are no longer uniformly distributed along the pipe.

Slug flow: the spherical cap bubbles coalescence with one another and with other smaller bubbles to form bigger ones, which almost fill the entire cross-section of the pipe resulting in higher void fraction. Consequently, the void fraction and bubble size at various places in the riser may become so high that bullet-shaped Taylor bubbles are formed as observed in Fig. 8 separated by slugs of silicone oil with some gas entrained in it as small bubbles. There are significant quantities of small bubbles in the liquid film surrounding the Taylor bubble.

Unstable slug: the flow pattern shown in Fig. 9 obtained at higher gas flow rates represents the transition to churn flow. An increase in gas coalescence in the liquid slug as a consequence of an increase in gas flow rate brought about oscillating of the liquid slug, thereby causing the liquid slug to begin to collapse.

Churn flow: as the gas flow rate increases further as shown in Fig. 10, the unstable slug flow regime ceases to exist as a result of breakdown of all of the liquid slugs. The breakdown slugs are now distributed in the form of waves on an annular film.

3.2.2. Flow regimes in bend (vertical 90° bend)

The two dominant factors governing the flow structure of a two-phase flow mixture in the 90° bends were the flow pattern as the mixture entered the bends and the interaction of gravitational and centrifugal forces.

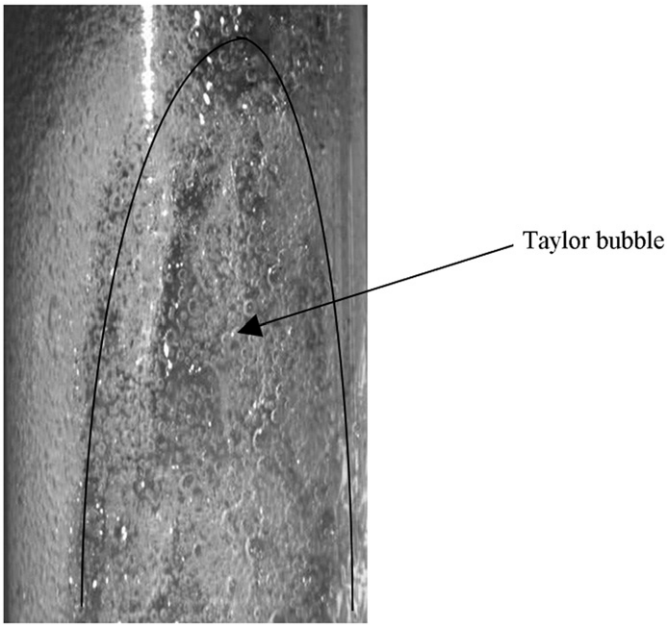

Fig. 8. Video image of slug flow for a riser at liquid and gas superficial velocities of 0.14 and 0.54 m/s, respectively.

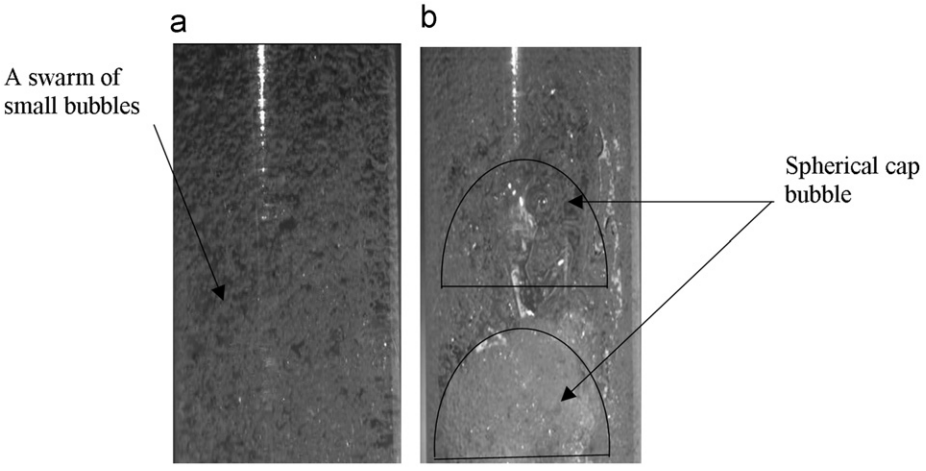

Fig. 7. Video image of spherical cap bubble for a riser at liquid and gas superficial velocities of 0.14 and 0.05 m/s, respectively.

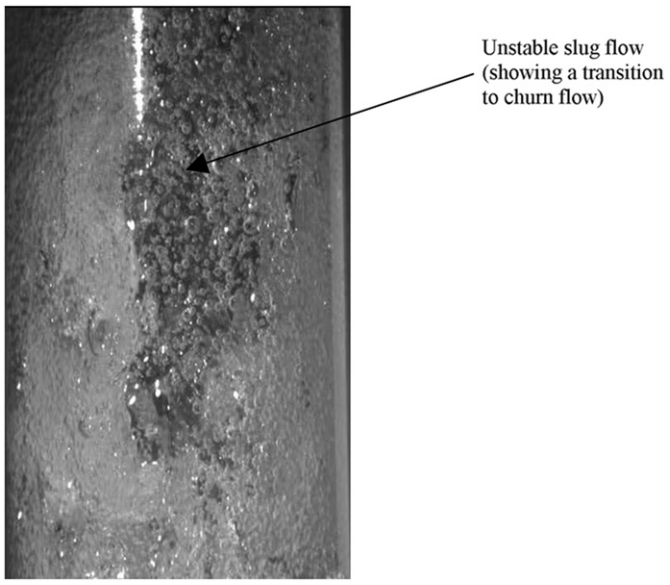

Fig. 9. Video image of unstable slug flow for a riser at liquid and gas superficial velocities of 0.14 and 0.95 m/s, respectively.

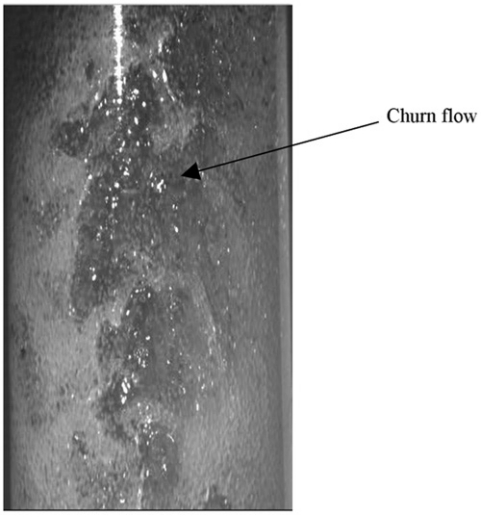

Fig. 10. Video image of churn flow for a riser at liquid and gas superficial velocities of 0.14 and 2.36 m/s, respectively.

When the flow pattern of the mixture entering the bend is spherical cap bubble with the size of the bubbles almost occupying the entire cross-section of the pipe, on entering the bend, the bubbles migrate to and follows outside the bend whilst the liquid moves to the inside of the bend as observed in Fig. 11a–c. Bigger bubbles are created as a consequence of high level of mixing. Some of the created bubbles as a result of low surface tension forces collapse almost immediately.

Slug and unstable flows: here the gravitational force dominates and the liquid moves to the inside of the bend whilst the Taylor bubbles to the outside of it as observed in Fig. 12a. The interesting thing that happened here is that as the Taylor bubble and liquid slug move up the bend, the liquid film in the annulus and liquid in the liquid slug starts to drain out and fall to the bottom of the bend. The falling liquid at the bottom of the bend with high momentum on the other hand, move in forward direction whilst the ones with lesser momentum move backward due to the shape of the curvature of the bend. The collapsed slug flow regime created a dry patch occupying almost 100% of the bend. This region, which is shown in Fig. 12b, is wetted periodically. According to Oshinowo and Charles (1974) unless there is a quick replenishment of the liquid plug as shown in Fig. 12c and d, the bend is liable to dry out, especially at the upper wall.

Churn flow: a different mechanism could be taking place for both the slug and churn flows. The centrifugal force dominates in this case, and the gas moves inside the bend. Because of the high shearing action of the gas on the gas–liquid interface, it picks some liquid whilst moving down and deposits them at the bottom of the bend and creates some droplet entrainment in the gas core. As a consequence of this we have liquid at both the top and bottom of the bend as observed in Fig. 13. However, some of the liquid at the top of the bend can be observed to drain down to the bottom of the bend. There was no dry patch observed in this regime.

Flow patterns just downstream of the bend can also be observed in the output of WMS as illustrated in Fig. 14.

3.2.3. *Flow patterns in the upstream flowline (horizontal 90° bend)*

For flowline (horizontal), a different classification had to be established; because gravity introduces an asymmetry into the flow: the density difference between both phases causes the liquid to travel preferentially along the bottom of the pipe. These flow patterns are described below in order of increasing gas flow rate.

Plug flow: the effect of gravity cause the gas plugs to move along the top of the pipe. The level of liquid in the pipe is usually higher than half the pipe.

Slug flow: this regime is characterized by the intermittent appearance of slugs of liquid, which bridge the entire pipe section and move at almost the gas velocity. It is typified by significant pressure fluctuations that occur. The length of the large bubble decreases with increase in gas flow rate for a given constant liquid flow rate.

Stratified wavy flow: at higher gas velocities within this flow pattern, the shearing action of the gas at the interface generates large amplitude waves on the liquid surface. Liquid is torn from the surface of these waves giving rise to drop entrainment in the gas region. These drops deposit partially on the top of the pipe.

3.2.4. *Flow patterns in the bend (horizontal 90° bend)*

Plug flow: the gas bubbles initially migrate towards the inner radius of the bend under the influence of centrifugal force, but subsequently it is forced outward due to the increasing effect of gravity.

Slug flow: at higher gas flow rate, the centrifugal force moves the liquid to the outside of the bend whilst the gas to the inside of the bend. The gravity force then takes the liquid to the inside of the bend and the gas to the outside of the bend. Only a little amount of liquid film drained downwards to the bottom of the bend. This behaviour was contrary to that observed for the slug flow in the vertical 90° bend.

Stratified wavy flow: the level of liquid in the pipe has dropped to less than half the diameter of the pipe with an increase in gas flow rate leading to collapse of bigger bubbles existing in the bend.

3.3. *Cross-sectional mean void fraction*

Mean void fraction was obtained by averaging the cross-sectional void fraction data over an interval of 60 s at a data acquisition frequency of 1000 Hz. This parameter is a good indicator for the general picture of phase distribution. The change of flow patterns can be qualitatively revealed by the variation of the variable.

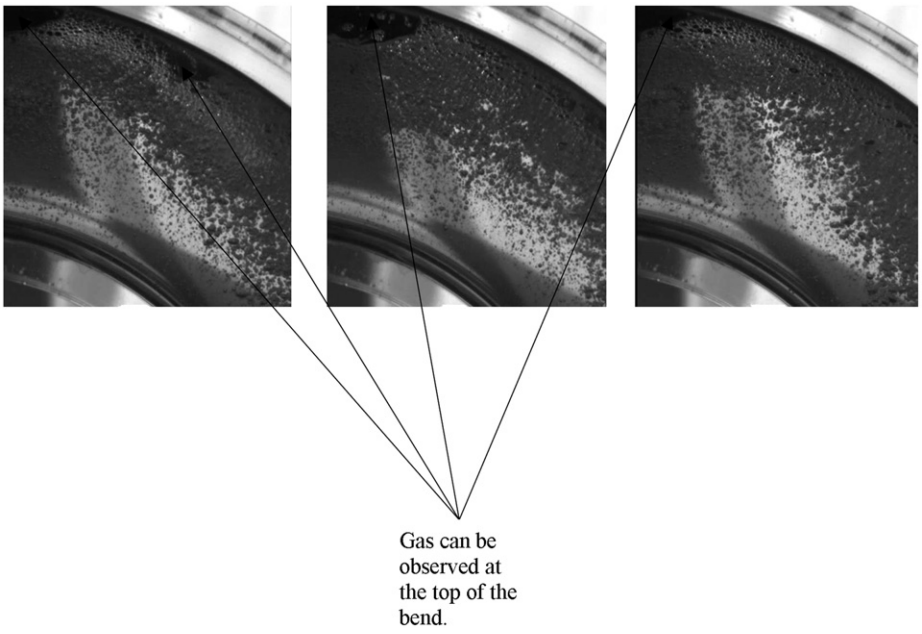

Fig. 11. Video image of spherical cap bubble flow passing through a vertical 90° bend at liquid and gas superficial velocities of 0.14 and 0.05 m/s, respectively.

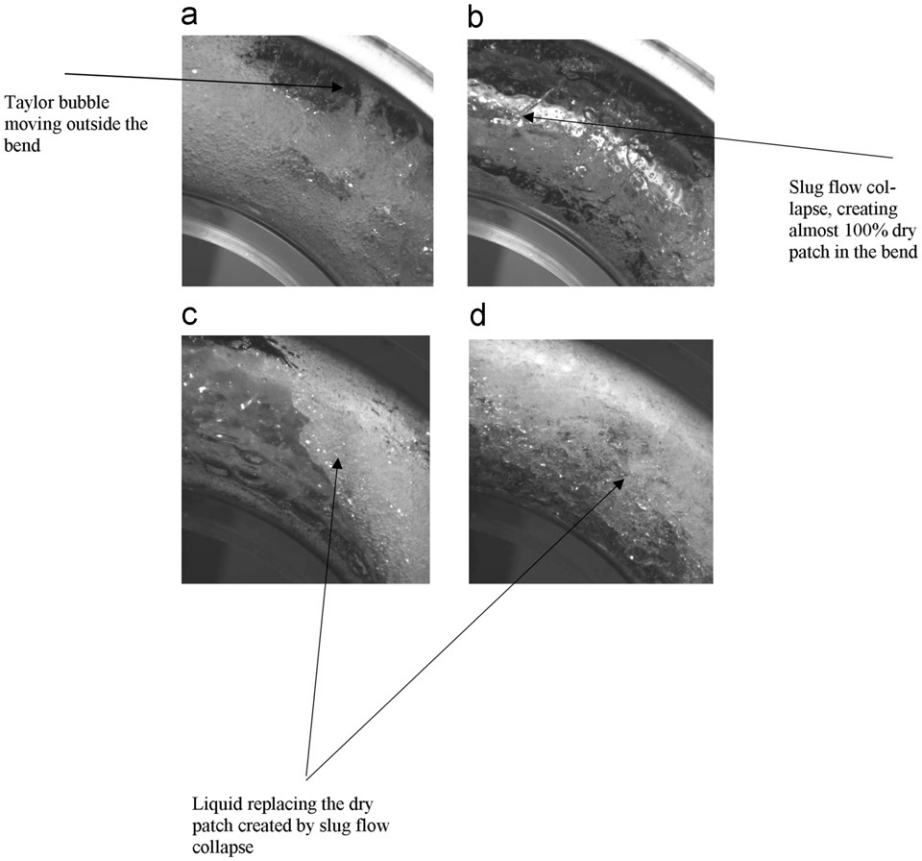

Fig. 12. Video image of slug flow passing through a vertical 90° bend at liquid and gas superficial velocities of 0.14 and 0.54 m/s, respectively.

3.3.1. The effect of gas superficial velocity

The effect of gas superficial velocity on the mean void fraction for the riser and flowline, before the vertical and horizontal 90° bends, respectively, is presented in Fig. 15. The mean void fraction increases monotonically with the gas superficial velocity but the increase at the lower gas superficial velocity is much sharper than that at the higher gas superficial velocity. At the lower and higher gas superficial velocities there is little difference in the mean void fraction for both the riser and flowline. This is not surprising because under these conditions the riser and flowline have more or less similar flow patterns as discussed in previous sections. In the intermediate gas flow rates (gas superficial velocity = 1–3 m/s) slight difference is observed owing to the different flow patterns developed in the two arrangements.

This is not the case for the situations after the bend. The mean void fraction after the bend for the vertical and horizontal 90° bends arrangements is shown in Fig. 16. Clearly the flowline, after the vertical 90° bend arrangement has considerably higher mean void fractions than those of the flowline setup, after the horizontal 90° bend for all the three liquid flow rates. The dominant flow pattern after the horizontal 90° bend is the stratified wavy flow whilst the slug, stratified and semi-annular flow are observed after the vertical 90° bend. The different flow patterns result in the different mean void fractions.

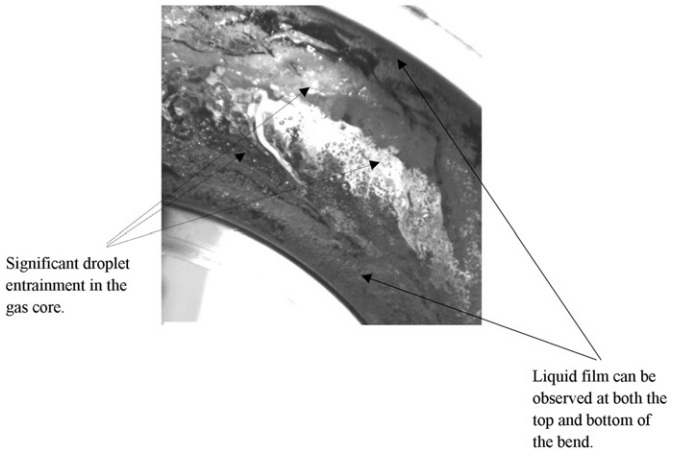

Fig. 13. Video image of churn flow passing through a vertical 90° bend at liquid and gas superficial velocities of 0.14 and 2.36 m/s, respectively.

3.3.2. *The effect of liquid superficial velocity*

Fig. 17 presents the effect of liquid superficial velocity on the mean void fraction in the riser and flowline, before the vertical and horizontal 90° bends. Generally, the mean void fractions in both the riser and the flowline decrease with an increase in liquid superficial velocity except at the higher gas superficial velocity (2.36 m/s) in the flowline where the mean void fraction slightly increases. The mean void fractions before the horizontal 90° bend at the lower liquid superficial velocity drop more significantly than those before the vertical 90° bend and then they become closer at the higher liquid superficial velocity. This is probably because in the examined range of gas superficial velocity, the influence of the liquid superficial velocity on the flow patterns is limited.

The effect of liquid superficial velocity on the mean void fractions after the vertical 90° bend is different from that after the horizontal 90° bend as shown in Fig. 18. The dependence of the mean void fractions after the vertical 90° bend on liquid superficial velocity is strongly influenced by gas superficial velocity. At low gas superficial velocity (0.05 m/s), the mean void

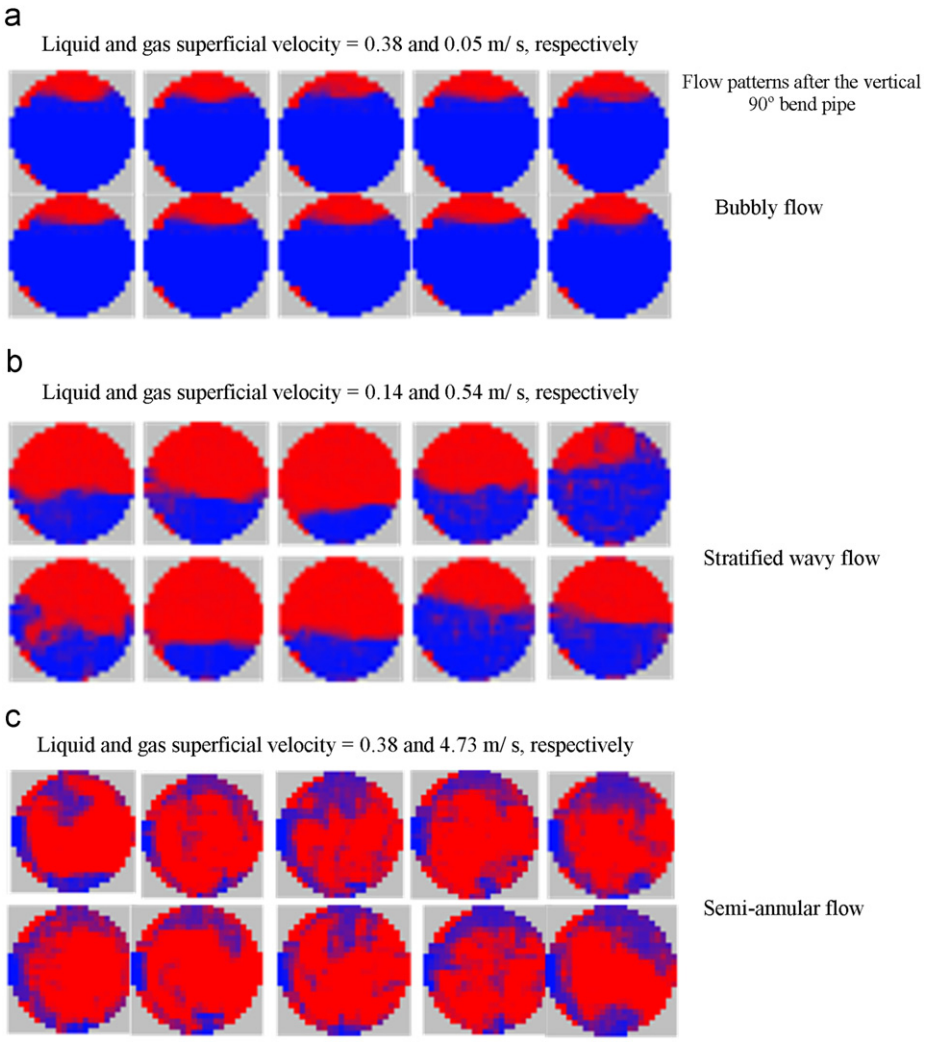

Fig. 14. Sequence of frames at 1 ms intervals showing the location of the gas, top and bottom of the pipe.

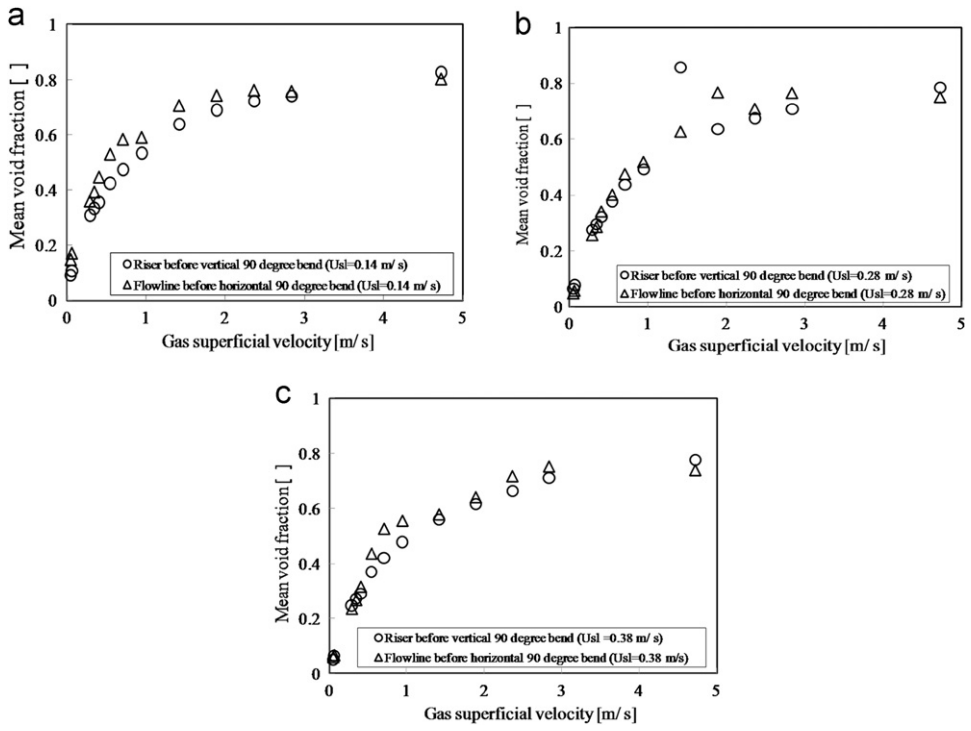

Fig. 15. Influence of gas superficial velocity on mean void fraction before vertical and horizontal 90° bends (liquid superficial velocity = 0.14, 0.28 and 0.38 m/s).

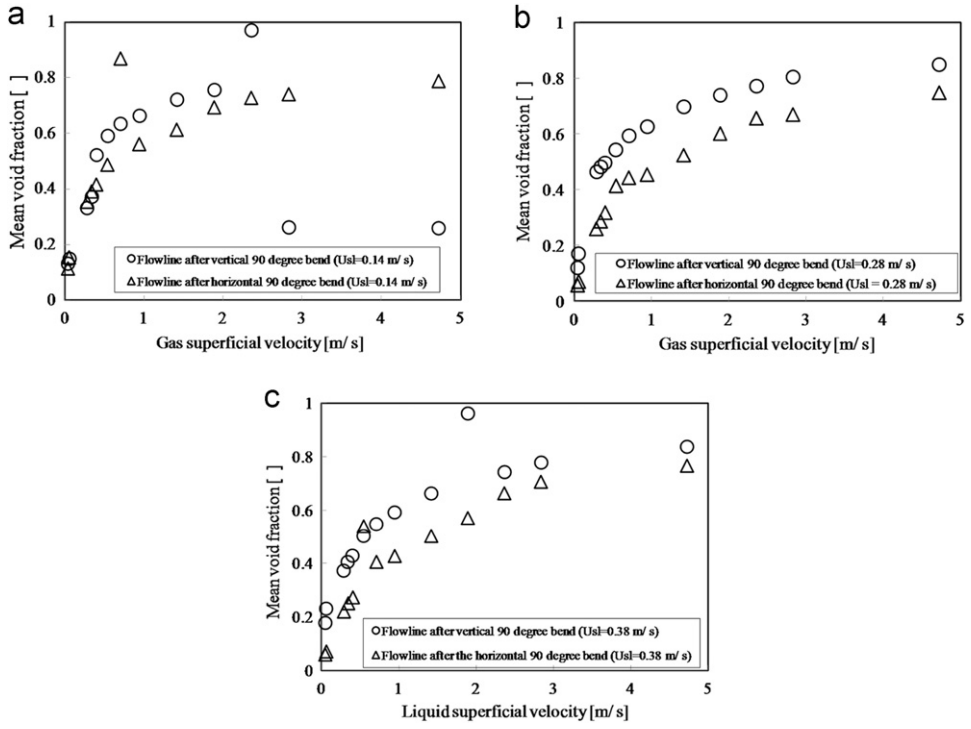

Fig. 16. Influence of gas superficial velocity on mean void fraction after vertical and horizontal 90° bends (liquid superficial velocity = 0.14, 0.28 and 0.38 m/s).

fraction decreases, changes a little and then increase with an increase in liquid superficial velocity. The opposite trend is shown for a gas superficial velocity of 0.40 m/s, the mean void fraction increases, changes a little and then decreases with an increase in liquid superficial velocity from the examined liquid superficial velocity range. The trend for gas superficial velocity at 2.36 m/s was similar to that for 0.40 m/s, but the mean void fraction decreases more sharply with an increase of liquid superficial velocity at the intermediate liquid superficial velocity. A general monotonic decrease trend was observed for the mean void fraction after the horizontal 90° bend with an increase in gas superficial velocity. These differences may be attributed to the

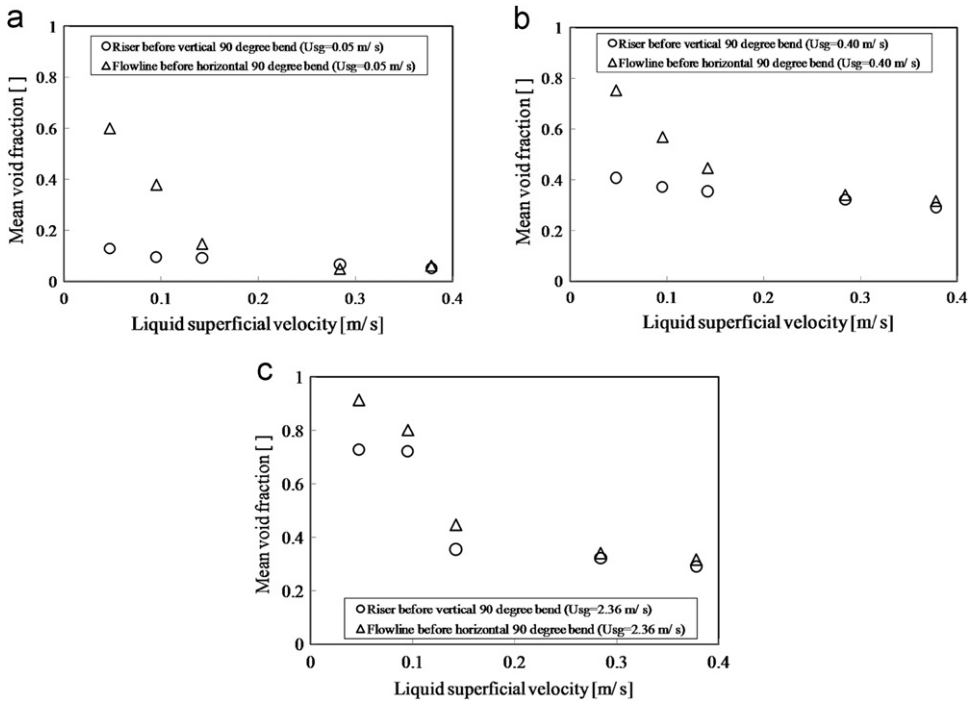

Fig. 17. Influence of liquid superficial velocity on mean void fraction before vertical and horizontal 90° bends (gas superficial velocity = 0.05, 0.40 and 2.36 m/s).

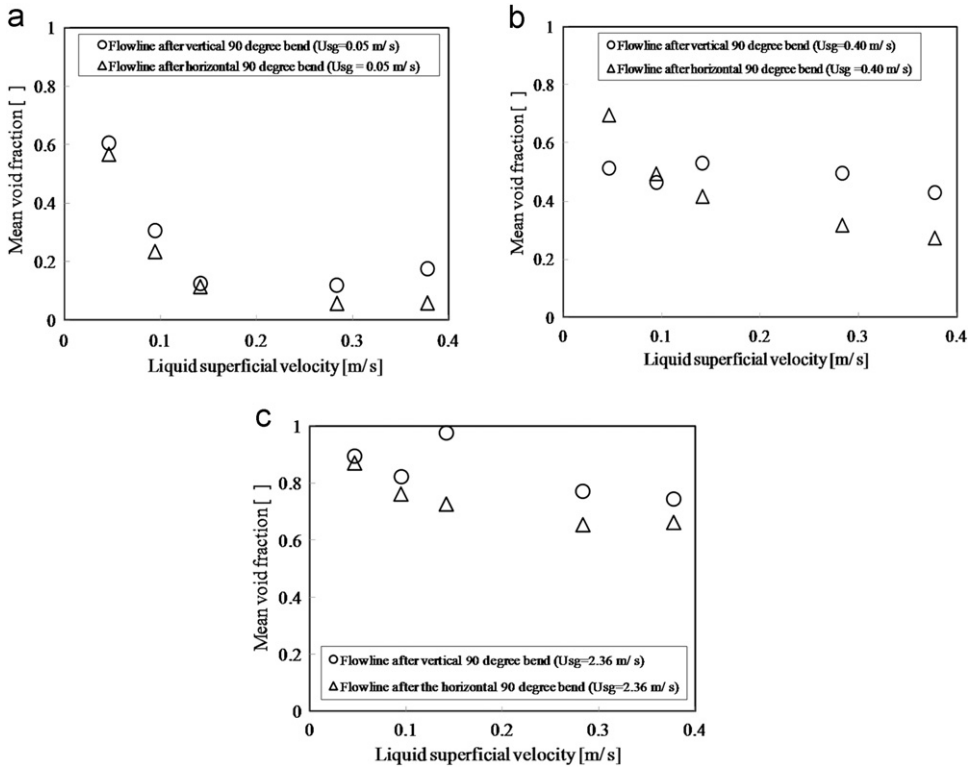

Fig. 18. Influence of liquid superficial velocity on mean void fraction after the vertical and horizontal 90° bends (gas superficial velocity = 0.05, 0.40 and 2.36 m/s).

change of flow patterns that resulted as a consequence of different gas and liquid superficial velocities but more detail analysis is needed to draw a conclusion.

3.4. Competition between centrifugal and gravitational forces

Gardner and Neller (1969) proposed a criterion based on a modified Froude number, F_r, to determine stratification after the bend. According to their proposed criterion, when F_r is greater than unity, the air will hug to the inside of the bend whilst for F_r less than unity, the air will move to the outside of the bend. The validity of the criterion will be discussed here.

The conditions for which the liquid goes to the outside or inside of the bend are identified in Fig. 19 as the Froude number is plotted against gas superficial velocity with liquid superficial velocity as a parameter. There was one combination of flow rate

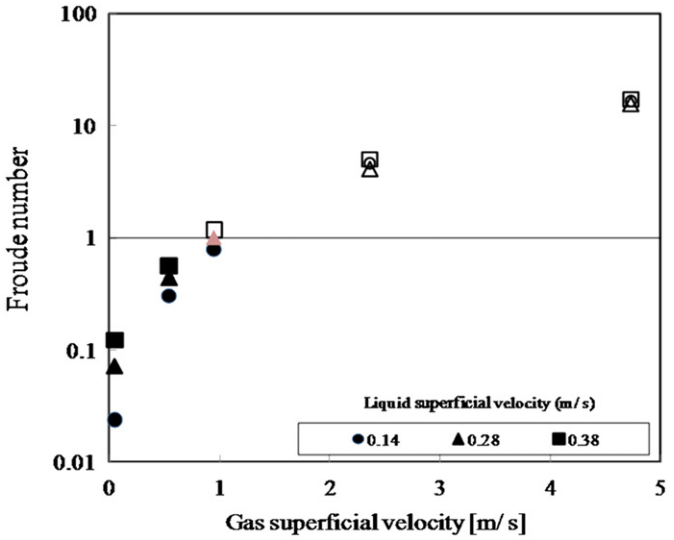

Fig. 19. Influence of gas superficial velocity on the modified Froude number with liquid superficial velocity as a parameter.

where it was not clear whether it was liquid or gas, which was on the outside of the bend. For flow rates which give a low Froude number, the flow patterns in the vertical pipe approaching the bend are cap bubble, slug and unstable slug flow. The gas superficial velocity is slightly greater than that for the liquid. As the liquid density is much greater than that for the gas and since $gR\sin\theta > U_m^2$, gravity dominates and we would expect the liquid to move to the inside of the bend, according to the fact observed in Figs. 11, 12 and 14a,b. In contrast, for churn flow, the gas superficial velocity is much greater than that for the liquid. Again the liquid density is much greater than that for the gas, the modified Froude number is greater than 1 and we would expect the liquid to move to the outside of the bend, according to the fact observed in Figs. 13 and 14c. The situation is further complicated by the fact that the centrifugal force acting on the fluid depends not only on the fluid velocity but also on the fluid density.

4. Conclusions

The effect of bends on two-phase gas–liquid flow has been successfully interrogated using advanced instrumentation, ECT and WMS. WMS has 24×24 steel wires with 0.12 mm diameter and measures the cross-sectional void fractions at 440 locations. The data were taken at an acquisition frequency of 200 and 1000 Hz for ECT and WMS, respectively, over an interval of 60 s. The characteristic signatures of Probability Density Function derived from the time series of cross-sectionally averaged void fraction data were used to identify the flow patterns. The results were validated by the analysis of the recorded high speed video images. The examined ranges of gas and liquid superficial velocities are 0.05–4.73 and 0.05–0.38 m/s, respectively. We have found that:

(1) ECT and WMS predicted same flow pattern signatures.
(2) With an increase in gas superficial velocity from 0.05 to 4.73 m/s, spherical cap bubble, slug, unstable slug and churn flows were observed in the vertical riser while in the horizontal flowline, plug, slug stratified wavy and annular flows were developed. Certainly buoyancy force plays an important role in the formation of the different flow patterns.
(3) Bends have significant effect on the gas–liquid flow. In both the vertical and horizontal 90° bends gravitational force tends to move the liquid to the inside of the bend while the gas to the outside of the bend. Some big spherical cap bubble and Taylor bubbles break up in the bends due to the balance of the centrifugal and the surface tension forces. The bubbles become more uniform. Dryness patch in the bend was observed in the slug and unstable slug flows. As a result, after the vertical bend the spherical cap bubble flow became bubbly flow, stable and unstable slug to stratified wavy flows and the churn flow turn to stratified wavy and semi-annular flows. The horizontal bend has less effect on the flow patterns compared with the vertical bend.
(4) At low liquid and high gas superficial velocities, both the vertical and horizontal 90° bends have the same effect on the two-phase air–silicone oil flow, the flow pattern downstream of the bend is annular.
(5) No slug flow was observed at low liquid flow rate both for the upstream and downstream sections of the horizontal 90° bend.
(6) Generally the mean void fraction was found to increase monotonically with gas superficial velocity before and after the bend. Little difference in the mean void fractions for the riser and flowline before the bend were detected whilst the mean void fractions after the vertical bend are significantly higher than those after the horizontal bend. The effect of the liquid superficial velocity on the mean void fraction is more complicated. More work is needed before any concrete conclusion can be drawn.
(7) Gardner and Neller (1969) proposed a criterion based on a modified Froude number ($Fr_\theta = U_m^2/Rg\sin\theta = 1$) to determine stratification after the bend. The present results confirm the validity of the criterion for a liquid of surface tension and viscosity different from those used by Gardner and Neller (1969).

Acknowledgements

M. Abdulkadir would like to express sincere appreciation to the Nigerian Government through the Petroleum Technology Development Fund (PTDF) for providing the funding for his doctoral studies.

Donglin Zhao and Safa Sharaf are funded by EPSRC under Grants EP/E004644/1 and EP/F016050/1.

This work has been undertaken within the Joint Project on Transient Multiphase Flows and Flow Assurance. The Author(s) wish to acknowledge the contributions made to this project by the UK Engineering and Physical Sciences Research Council (EPSRC) and the following: – GL Industrial Services; BP Exploration; CD-adapco; Chevron; ConocoPhillips; ENI; ExxonMobil; FEESA; IFP; Institutt for Energiteknikk; PDVSA (INTEVEP); Petrobras; PETRONAS; SPT; Shell; SINTEF; Statoil and TOTAL. The Author(s) wish to express their sincere gratitude for this support.

References

Abdulkadir, M., Hernandez-Perez, V., Sharaf, S., Lowndes, I.S., Azzopardi, B.J., 2010. Experimental investigation of phase distributions of an air–silicone oil flow in a vertical pipe. World Academy of Science, Engineering and Technology 61, 52–59.

Azzi, A., Friedel, L., 2005. Two-Phase upward flow 90 degree bend pressure loss model. Forschung im Ingenieurwasen 69, 120–130.

Azzi, A., Friedel, L., Kibboua, R., Shannak, B., 2002. Reproductive accuracy of two-phase flow pressure loss correlations for vertical 90 degree bends. Forschung im Ingenieurwasen 67, 109–116.

Carver, M.B., 1984. Numerical computation of phase separation in two fluid flow. ASME Journal of Fluids Engineering 106, 147–153.

Carver, M.B., Salcudean, M., 1986. Three-dimensional numerical modelling of phase distribution of two-fluid flow in elbows and return bends. Numerical Heat Transfer 10, 229–251.

Costigan, G., Whalley, P.B., 1996. Slug flow regime identification from dynamic void fraction measurements in vertical air-water flows. International Journal of Multiphase Flow 23, 263–282.

da Silva, M.J., Thiele, S., Abdulkareem, L., Azzopardi, B.J., Hampel, U., 2010. High-resolution gas–oil two-phase flow visualization with a capacitance wire-mesh sensor. Flow Measurement and Instrumentation 21, 191–197.

Dean, W.R., 1927. Note on the motion of a fluid in a curved pipe. Philosophical Magazine 4, 208–223.

Dean, W.R., 1928. Stream-line motion of a fluid in a curved pipe. Philosophical Magazine 5, 673–695.

Dewhurst, S.J., Martin, S.R., Jayanti, S., Costigan, G., 1990. Flow Measurements Using 3-D LDA System in a Square Section 90 Degree Bend. Report AEA-In Tech-0078.

Ellul, I.R., Issa, R.I., 1987. Prediction of the flow of interspersed gas and liquid phases through pipe bends. Transaction of Institution of Chemical Engineers 65, 84–96.

Eustice, J., 1910. Flow of water in curved pipes. Proceedings of the Royal Society A 84, 107–118.

Gardner, G.C., Neller, P.H., 1969. Phase distributions flow of an air–water mixture round bends and past obstructions. Proceedings of the Institution of Mechanical Engineers 184, 93–101.

Hammer, E.A., 1983. Three-component Flow Measurement In Oil/Gas/Water Mixtures Using Capacitance Transducers, Ph.D. Thesis, University of Manchester.

Hernandez Perez, V., Azzopardi, B.J., Kaji, R., daSilva, M.J., Beyer, M., Hampel, U., 2010. Wisp-like structures invertical gas–liquid pipe flow revealed by Wire Mesh Sensor studies. International Journal of Multiphase Flow 36, 908–915.

Huang, S.M., 1995. Impedance sensors-dielectric systems. In: Williams, R.A., Beck, M.S. (Eds.), Process Tomography. Butterworth-Heinemann Ltd., Cornwall.

Hunt, A., Pendleton, J., Byars, M., 2004. Non-intrusive measurement of volume and mass using electrical capacitance tomography. In: Proceedings of the 7th Biennial ASME Conference on Engineering System Design and Analysis, Manchester, UK, ESDA 2004-58398.

Jayanti, S., 1990. Contribution to the Study Of Non-axisymmetric Flows. Ph.D. Thesis, Imperial College London.

Legius, H.J.W.M., van der Akker, H.E.A., 1997. Numerical and experimental analysis of translational gas–liquid pipe flow through a vertical bend. In: Proceedings of the 8th International Conference Multiphase (BHR) Group, Cannes, France, 18–20 June.

Oshinowo, T., Charles, M.E., 1974. Vertical two-phase flow-Part 1: flow pattern correlations. Canadian Journal of Chemical Engineering 52, 25–35.

Omebere-Iyari, N.K., Azzopardi, B.J., 2007. A study of flow patterns for gas/liquid flow in small diameter tubes. Chemical Engineering Research and Design 85, 180–192.

Shannak, B., Al-Shannag, M., Al-Anber, Z.A., 2009. Gas–liquid pressure drop in vertically wavy 90 degree bend. Experimental Thermal and Fluid Science 33, 340–347.

Spedding, P.L., Benard, E., 2006. Gas–liquid two-phase flow through a vertical 90 degree elbow bend. Experimental Thermal and Fluid Science 31, 761–769.

Spedding, P.L., Benard, E., McNally, G.M., 2004. Fluid flow through 90 degree bends. Development of Chemical Engineering Mineral Process 12, 107–128.

Zhu, K., Madhusudana Rao, S., Wang, C., Sundaresan, S., 2003. Electrical capacitance tomography measurements on vertical and inclined pneumatic conveying of granular solids. Chemical Engineering Science 58, 4225–4245.